Trade Science Inc.

ISSN : 0974 - 7443 Volume 6 Issue 2

CHEMICAL TECHNOLOGY

An Indian Journal

Full Paper

CTAIJ 6(2) 2011 [123-129]

Pressure field and energy distribution in froth flotation cell

Krishna Kumar, Subrata Kumar Majumder*

Department of Chemical Engineering, Indian Institute of Technology Guwahati, (INDIA)

E-mail: skmaju@iitg.ernet.in

Received: 17th May, 2011 ; Accepted: 17th June, 2011

ABSTRACT

Pressure drop and energy distribution are two important design parameters of a flotation cell. The energy distribution of phases in the flotation cell strongly influences the recovery of minerals by flotation process. Therefore, investigating these hydrodynamic characteristics is required to analyze the performance of the flotation process. In this work, the behaviors of pressure and kinetic energy distribution in a flotation cell have been analyzed by computational fluid dynamic simulation.

KEYWORDS

Froth flotation;
Pressure;
Kinetic energy;
Power number.

INTRODUCTION

Froth flotation is one of the important processes that widely used for mineral separation, for water treatment, de-inking of recycled paper and electrolyte cleaning (oil separation) applications[3]. Different authors have investigated different hydrodynamic characteristics in flotation cell[6,11]. Gorain and Franzidis[5] carried out studies on impeller type, impeller speed and air flow rate in an industrial scale flotation cell. Koh and Schwarz[8] studied the influences of bubble particle collision rates on the efficiencies of a flotation cell. Delgon and Meyer[4] studied the turbulent flow behavior of phases in flotation cell by Multiple Reference Frames (MRF) impeller rotation model and the standard k–ε turbulence model and concluded that it can accurately model turbulent fluid flow combining fine grids with higher–order discretization schemes. Panneerselvam and Savithri[10] analyses the same by using Eulerian–Eulerian multi-fluid approach along with standard k-ε turbulence model. The very recent study was carried out by Roy et al.[12] on flow structure and the effect of macro-instabilities in a pitched-blade stirred tank. From the literature it is found that most of the studies have been focused on analyzing the flow field but there is a study on pressure field and turbulent kinetic energy distribution in the flotation cell. In this work the pressure field and the kinetic energy distribution in the flotation cell has been analyzed by computational fluid dynamic simulation.

System considered in the present study

A cylindrical vessel of diameter of 2.5 m and a height of 3.05 m with semispherical bottom was considered as a flotation tank in this study. A four-bladed Pitched blade impeller pumping down (PBTD) with blades at an angle of 45o from the horizontal plane was considered as a provision to make intense mixing of phases in the tank. The volume of the tank is 15.0 m3. The diameter of the impeller was Da=T/2. The width and clearance of bottom were considered as l mm and C=T/3. Four baffles of T/10 in diameter were considered to equally place around the tank. The working material was water as liquid phase and air as gaseous phase. The rotation speed of the impeller was varied while

Full Paper

keeping gas velocity constant and on the other hand gas velocity was varied while keeping rotation velocity of the impeller constant. The schematic diagram of the flotation tank is shown Figure 1.

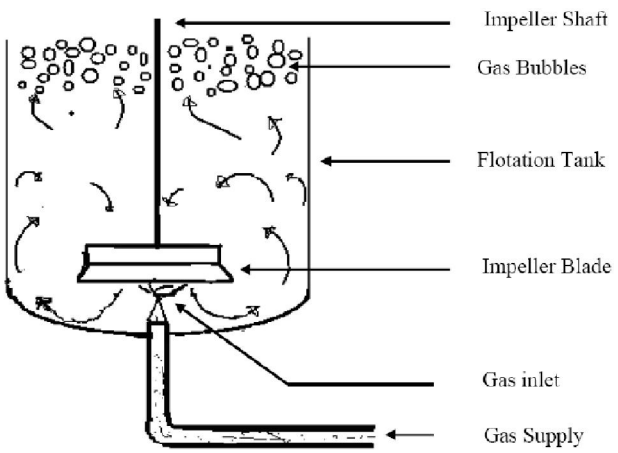

Figure 1 : Schematic diagram of a flotation cell

Gas is entering from bottom side of the tank. Due to the symmetry of the geometry, only one-fourth of the flotation cell is considered as the computational domain. The very first step in any CFD simulation is the discretization of the computational domain. In this study the geometry discretization is done using block structured grids which allows finer grids in regions where higher spatial resolutions are required. The computational grid used of its 1/4th section which has been used in this simulation work. The system properties which are considered in the present work are shown in TABLE 1.

TABLE 1 : Properties of system considered for this simulation work

Properties	Gas	Liquid
Thermal expansivity	0.003356 K^{-1}	2.57×10^{-4} K^{-1}
Dynamic viscosity	1.831×10^{-05} kg/m.s	8.899×10^{-4} kg/m s
Density	1.185 kg/m^3	997.0 kg/m^3
Molar mass	28.96 g/mol	18.02 kg/mol
Reference pressure	1 atm	1 atm
Reference Temperature	25^0 C	25^0 C
Reference specific enthalpy	0.0 J/kg	0.0 J/kg
Reference specific entropy	0.0 J/kg/K	0.0 J/kg/K
Specific heat capacity	1.0044×10^3 J/kg K	4181.7 J/kg K
Thermal conductivity	2.61×10^{-02} W/m	0.6069 W/m K

THEORETICAL BACKGROUND

Two distinct multiphase flow models are available. These are Eulerian–Eulerian multiphase model and a Lagrangian particle tracking multiphase model. Two different sub-models are available for Eulerian - Eulerian multiphase flow. These are homogeneous model and inter-fluid transfer (inhomogeneous) model. In present work, for gas phase Zero equation parameter model is employed whereas for liquid phase two equation model that is Standard k-ε model has been employed.

Two-equation model

Boussinesq hypothesis

$$-\rho\overline{u_i'u_j'} = -\rho\frac{2}{3}k\delta_{ij} + \left[\mu_t\left(\frac{\partial\overline{u_i}}{\partial x_j} + \frac{\partial\overline{u_j}}{\partial x_i}\right)\right] \quad (1)$$

Turbulent viscosity

$$\mu_t = \rho C_\mu \frac{k^2}{\varepsilon} \quad (2)$$

Standard k-ε model

In the Standard k-ε model the modeled transport equations for the k and ε.

Turbulent kinetic energy (k)

$$\underbrace{\rho U_i\frac{\partial k}{\partial x_i}}_{\text{Convection}} = \underbrace{\mu_t\left(\frac{\partial U_j}{\partial x_i} + \frac{\partial U_i}{\partial x_j}\right)\frac{\partial U_j}{\partial x_i}}_{\text{Generation}} + \underbrace{\frac{\partial}{\partial x_i}\left\{\left(\frac{\mu_t}{\sigma_\varepsilon}\right)\frac{\partial k}{\partial x_i}\right\}}_{\text{Diffusion}} - \underbrace{\rho\varepsilon}_{\text{Dissipation}} \quad (3)$$

Turbulent dissipation (Є)

$$\underbrace{\rho U_i\frac{\partial \varepsilon}{\partial x_i}}_{\text{Convection}} = \underbrace{C_{1\varepsilon}\left(\frac{\varepsilon}{k}\right)\mu_t\left(\frac{\partial U_j}{\partial x_i} + \frac{\partial U_i}{\partial x_j}\right)\frac{\partial U_j}{\partial x_i}}_{\text{Generation}} + \underbrace{\frac{\partial}{\partial x_i}\left\{\left(\frac{\mu_t}{\sigma_\varepsilon}\right)\frac{\partial \varepsilon}{\partial x_i}\right\}}_{\text{Diffusion}} - \underbrace{C_{2\varepsilon}\rho\frac{\varepsilon^2}{k}}_{\text{Destruction}} \quad (4)$$

where σ_k, σ_ε, $\sigma_{1\varepsilon}$, and $C_{2\varepsilon}$ are standard k-ε model constants. Using the standard k–e model the turbulent viscosity of the continuous phase is calculated by:

$$\mu_{\alpha,tur} = C_\mu\rho_c\frac{k_c^2}{\varepsilon_c} \quad (5)$$

For the continuous liquid phase, a k–ε model is applied with its standard constants: $C_{1\varepsilon}$ = 1.44, $C_{2\varepsilon}$ = 1.92, Cμ = 0:09; σ_k = 1 and σ_ε = 1.3. The effective viscosity is then

$$\mu_{\alpha,effec} = \mu_{\alpha,lam} + \frac{\mu_{\alpha,tur}}{\sigma_k} \quad (6)$$

Simulation procedure

The simulation is done using the commercial code provided by Ansys CFX software. A uniform velocity profile is assumed in the bottom side inlet. A control volume finite method is employed to solve the governing equations. k-ε model is used for capturing the turbulence of liquid for the given situation. Zero equation models have been employed for capturing the turbulence of gas phase for the given situation. As said in the theory k-ε is two parameter based model is sufficient enough for the situation. The mean gas bubble diameter of 3.0 mm is assumed for all our simulations. Further, the validity of bubble size used in the CFD simulation is validated by calculating the bubble size based on the reported correlations in literature[1] by using the simulation results of gas holdup and power consumption values.

Boundary conditions

(i) an inlet through which air enters the mixer. Inlet: Speed = 5 m/s; Static Temperature = 25° C (ii) A degassing outlet, so that only the gas phase can leave the domain. Boundary type = outlet; Location = upper liquid surface, Boundary details = Degassing condition. (iii) Thin surfaces for the baffle and impeller blade. In ANSYS CFX-Pre, thin surfaces can be created by specifying wall boundary conditions on both sides of internal 2D regions. Both sides of the baffle regions will be specified as walls in this case. Boundary Type = Wall; Location = Wall Baffles. For air at 25° C, wall influence on flow is taken as free slip. For water, wall influence on flow is taken as no slip. Here the wall baffles region includes the surfaces on both sides of the baffle. Therefore, we do not need to use the Create Thin Surface Partner (CTSP) option. The free slip condition can be used for the gas phase since the contact area with the walls is near zero for low gas phase volume fractions. (iv) A wall for the hub and shaft in the rotating domain. This will be stationary relative to the rotating domain. These regions are connected to the shaft in the impeller domain. Since the tank domain is not rotating, we need to specify a moving wall to account for the rotation of the shaft. Part of the shaft is located directly above the air inlet, so the volume fraction of air in this location will be high and the assumption of zero contact area for the gas phase is not physically correct. In this case, a no slip boundary condition is more appropriate than a free slip condition for the air phase. When the volume fraction of air in contact with a wall is low, a free slip condition is more appropriate for the air phase. Axis of rotation was taken in X-direction, (v) A wall for the shaft in the stationary domain. This will be rotating relative to the stationary domain. Boundary Type = Wall; Location = Blade, Hub, Shaft. For air at 25° C, wall influence on flow is taken as free slip. For water, wall influence on flow is taken as no slip, (vi) periodic domain interfaces for the periodic faces of the tank and impeller. (vii) Initial values: The initialization for volume fraction is 0 for air. Therefore, the initial volume fraction for water will be set to 1 so that the sum of the two fluid volume fractions is 1. Initial water velocity is taken as 0 m/s.

Convergence control properties

Turbulent eddy dissipation is incorporated in the simulation. Blend factor of 0.75 is employed as our advection scheme in the solver. Timescale Control= 1 s. Max Number of Iterations = 3000. Residual Type=RMS. Residual Target=10^{-10}

RESULTS AND DISCUSSION

In this section, the variation of pressure and the kinetic energy distribution have been interpreted based on the rotational speed of impeller and the gas velocity in the flotation cell.

Pressure profile

Contour for pressure distribution is shown in Figure 2 and Figure 3. Figure 2 presents contour plot of pressure field inside the flotation tank for different values of inlet gas flow rate into the tank at constant rotational velocity, N=100 rpm, of impeller. It is notable that the hydrostatic contribution to pressure is excluded due to the use of an appropriate buoyancy reference density. From the figure it can be clearly seen that there are two high pressure zones present, one is at the surface of liquid in flotation tank while the other is observed near the corner of the dished bottom and the minimum pressure zone is present in vicinity of the im-

Full Paper

peller blades. It may be because of presence of high velocity zone for both gas and liquid resides in vicinity of impeller's blade. As distance from impeller's blade increases magnitude of velocity vector for both gas and liquid decreases, therefore pressure increases in either side of the impeller. As the gassing rate increases into the tank the pressure range into the tank increases and the pressure in the low pressure zone which is near to impeller blades also increases. At low gas flow rates, the vortex cavity regime is observed, while at higher gas flow rates, ventilated gas cavities form which extends to the blade surface, referred to as the large cavity regimes which are basically the lower pressure regions. Similar observations were reported by Warmoeskerken and Smith[14]. According to them in gas-sparged tanks, gas cavities form in the low-pressure region on the trailing side of impeller blades. This is the good qualitative agreement. Figure 3 presents the contour of pressure field inside the flotation tank for different values of rotational velocity of impeller at constant inlet gas flow rate, v_g = 5 m/s, into the tank. Figure 3 depicts that there are two high pressure zones present; one is at the surface of liquid in flotation tank while the other is observed near the corner of the dished bottom and the minimum pressure zone is present in vicinity of the impeller blades. The pressure in the low pressure zone decreases by increasing the impeller rotational speed which is opposite to the other case of high pressure zone. This is due to increase in rotational speed causes higher degree of turbulence that is high velocity fluctuation leads to large low pressure region which are also known as gas cavity. However due to the unavailability of the numerical data for pressure field inside the tank validation of current data is not possible. Therefore this analysis of the pressure field is kept as qualitative analysis. Experimental observations should be performed to validate the pressure distribution data.

Turbulent kinetic energy profile

A CFD model should be able to predict turbulence parameters such as RMS fluctuating velocities or turbulent kinetic energy in a stirred tank. As already noted, computational fluid dynamics models generally predict mean fluid velocities in the tank with reasonable accu-

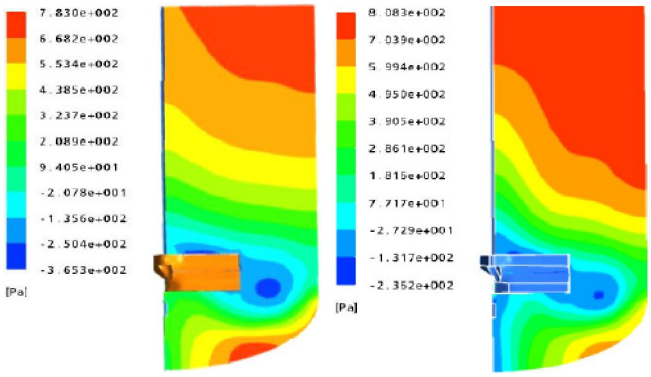

(a) v_g = 2 m/s (b) v_g = 5 m/s

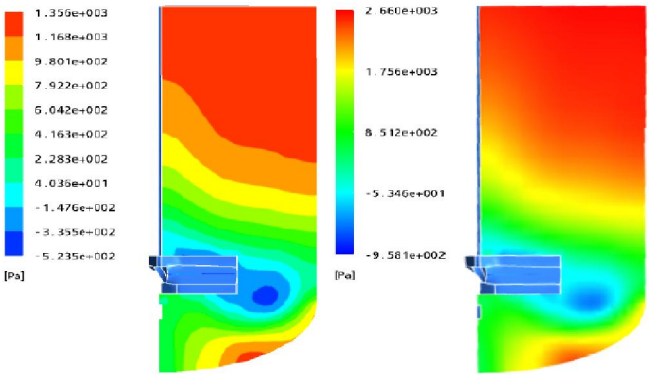

(a) N = 110 rpm (b) N = 150 rpm

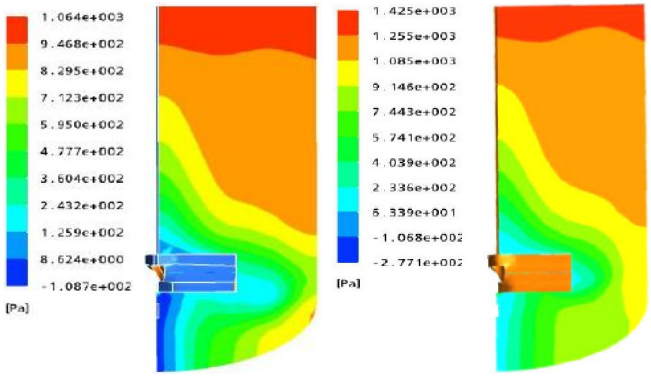

(c) v_g = 7.5 m/s (d) v_g = 12 m/s

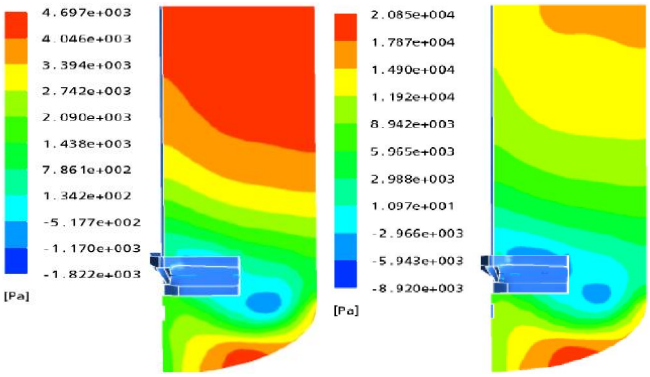

(c) N = 200 rpm (d) N = 400 rpm

Figure 2 : Contour plot of pressure field at constant rotational velocity, N=100 rpm, of impeller.

Figure 3 : Contour of pressure field at constant inlet gas flow rate, v_g =5 m/s.

racy but it leads to over or under prediction of turbulence quantities. Therefore, turbulence is the problematic area in fluid dynamics. This is often attributed to deficiencies in the models for the turbulence. Figure 4 and 5 illustrate the spatial distribution of turbulent kinetic energy. If k as a measure of the energy dissipation in the stirred vessel, one may see that greatest on the lower side of the impeller near the tip, where the radial velocity is also the greatest. An overall lower distribution of turbulent kinetic energy (k) can be observed on the upper side of the impeller where the average velocities are more uniform.

Figure 4 presents the contour plot of turbulent kinetic energy (k) field inside the flotation tank for different values of inlet gas flow rate into the tank at constant rotational speed, N=100 rpm, of impeller. Figure 5 shows the contour of turbulent kinetic energy (k) field inside the flotation tank for different values of rotational velocity of impeller at constant inlet gas flow rate, v_g =5m/s into the tank. In both the cases the kinetic energy is high along the impeller jet-stream and shows a peak at the trailing edge vortex location. Schafer et al.[13] observed similar kind of behavior of turbulent kinetic energy (k) in the vicinity of trailing edge vortices for pitched blade impeller. The second

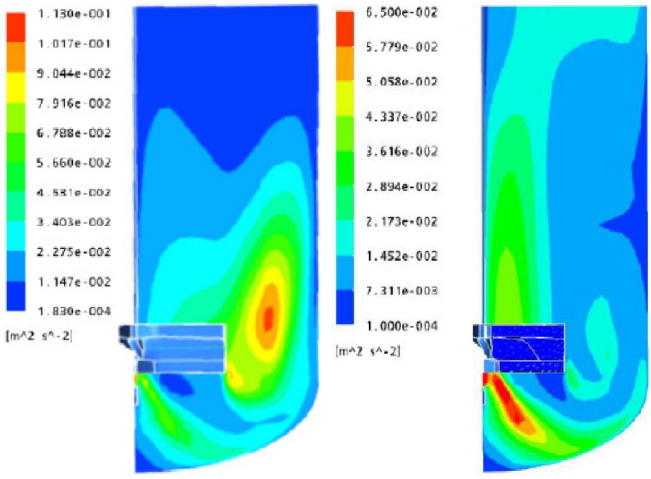

(a) v_g = 2 m/s (b) v_g = 5 m/s

Figure 4 : Contour plot of turbulent kinetic energy (k) field at constant N = 100 rpm.

significant peak of kinetic energy is observed near the corner of the dished bottom which can be attributed to the secondary circulation set in by the impeller jet stream hitting the tank corner.

Although no significant enhancement is observed in these levels of turbulent kinetic energy with increases in impeller speed (i.e., Reynolds number), for N = 400 rpm, a higher kinetic energy near the secondary circulation is observed which may be due to the fact that axial pumping increases with increase in rotational speed of the impeller and the enhancement in axial velocity forms a stronger corner vortex. The similar sort of behavior was also observed by Roy et al.[12]. Levels of turbulent kinetic energy are qualitatively well predicted in the vicinity of the impeller, an over-prediction of 7.69% in turbulent kinetic energy was observed for rotational speed, N=150 rpm, this was compared with the data provided by Roy et al[12].

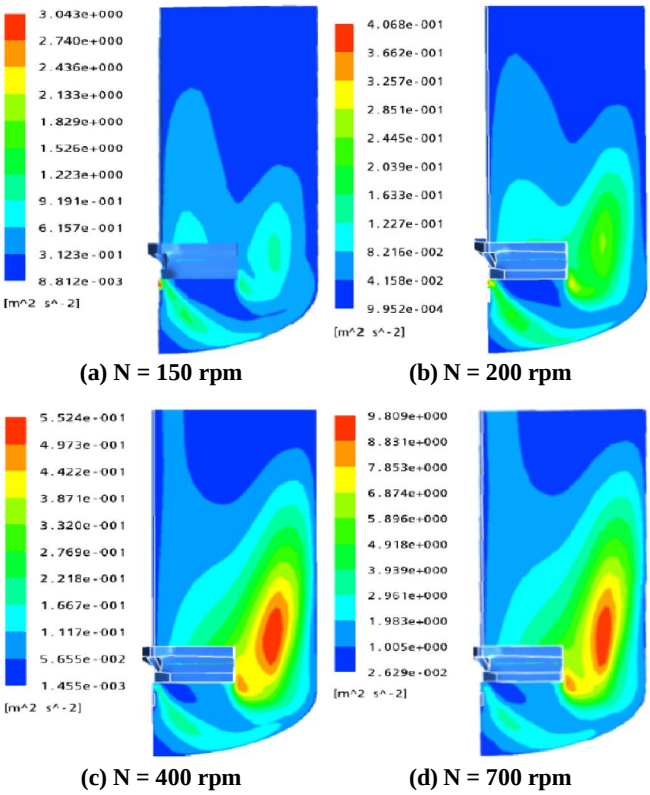

(a) N = 150 rpm (b) N = 200 rpm

(c) N = 400 rpm (d) N = 700 rpm

Figure 5 : Contour of turbulent kinetic energy (k) field at, v_g = 5 m/s into the tank.

Power number variation

Power number is the most important factor for characterizing the gross flow field characteristics of the mechanically agitated flotation cell.At industrial level, the rate of energy consumption per unit volume of fluid is used extensively for scale-up, scale-down and design purposes. Although it is widely used, the dependence of rate of energy consumption on impeller and tank geometry is defined only in the most general terms.

Full Paper

This is generally due to the difficulty of obtaining accurate torque value measurements on the small scale, and partly due to the predictive limitations of drag theory, particularly for recalculating three dimensional flows[2]. By the use of dimensional analysis, power number can be expressed as:

$$N_p = \frac{P}{\rho N^3 D_a^5} \quad (7)$$

where P is the power required by the impeller, ρ is the fluid density, N is the rotating speed of the impeller in rotation per second, and D_a is the diameter of the impeller. The power is usually calculated from measurements of the torque and the shaft speed of impeller.

$$P = 2\pi N T_q \quad (8)$$

where T_q is the sum of the torque acting on the both sides of the impeller blades, Hub shaft and tank shaft. The dependence of power number on Reynolds number (Re) is analogous to well established result for the friction factor in pipe flow, and for the drag coefficient on a sphere. In the laminar range (Re < 10 to 100, depending on the impeller of interest), the power number is inversely proportional to the Reynolds number ($N_p \propto 1/Re$). In the fully turbulent range (Re > 2×10^4), the power number is constant and independent of the Reynolds number[2]. In this work, torque was calculated for different values of impeller rotation speed from 1 rpm to 700 rpm. The values calculated for the power requirement for the work done is on the fluid only, it does not account for any mechanical losses, efficiencies etc. Also note that the accuracy of these results is significantly affected by the coarseness of the mesh. The range of Reynolds numbers considered extends well down into the transitional range for pitched blade impeller. The power number is first decreasing with the Reynolds number and after crossing a particular Reynolds number it increases very slightly and then finally becomes constant as shown in Figure 6.

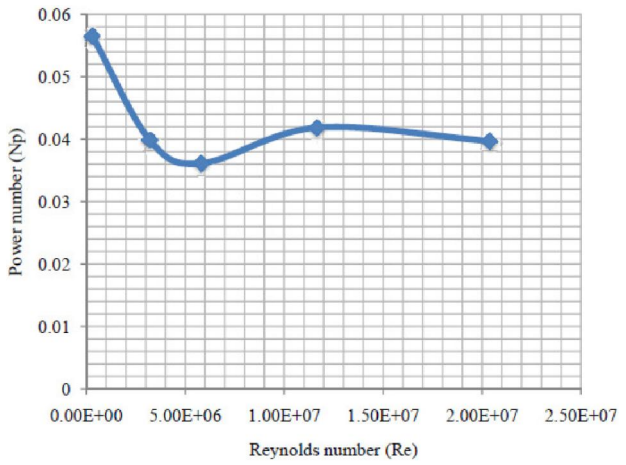

Figure 6 : Variation of power number (NP) with Reynolds number.

This sudden drop in power number is associated with the abrupt transition in the flow pattern from a radial to an axial flow Hockey et al.[7] and was quantified by the velocity measurements of Nouri and Whitelaw[9]. The power per unit volume required for the dispersion of phases in the flotation tank is shown in TABLE 2

TABLE 2 : Variations of power per unit volume required for dispersion of phases inside the tank.

Re ×10^{-5} (-)	N_p (-), $N_p = P/\rho N^3 D_a^5$	N (r/s)	P (W)	P/V (W/m^3)
32.09	0.03987	0.167	0.57	0.04
58.35	0.036136	1.67	513.61	34.24
116.70	0.041856	2.50	1995.85	133.06
204.23	0.039693	3.33	4472.97	298.20
229.03	0.033282	6.67	30139.97	2009.33

NOTATIONS

C_μ, $C_{\varepsilon 1}$, $C_{\varepsilon 2}$	:	constants in k–ε model
C_1, C_2	:	constants
k	:	turb. kinetic energy (m^2/s^2)
NP	:	power number (-)
P	:	pressure (N/m^2)
P	:	power (N.m/s)
Re	:	Reynolds number
S	:	source term, various
u,v	:	velocity (m/s)
ρ	:	density (kg/m^3)
ε	:	turb. dissipation rate (m^2/s^3)
μ	:	viscosity (kg/m s)
σ	:	constants in k–ε model
υ	:	kinematic viscosity (m2/s)
i, j	:	spatial directions
T	:	tank diameter (m)
T_q	:	torque (N.m/s)
H	:	tank height (m)
D_a	:	impeller diameter (m)
d_b	:	mean bubble diameter (m)
v_g	:	gas inlet flow rate (m/s)

N : rotation speed of impeller
U_t : turbulent velocity scale

CONCLUSION

Pressure variation and the kinetic energy distribution inside the flotation tank for different values of gas velocity have been enunciated in the present work. From the analysis it is concluded that as the gas flow rate increases into the tank the pressure range into the tank increases and the pressure in the low pressure zone which is near to impeller blades also increases. The vortex cavity regime are the results of low gas flow rates whereas higher gas flow rates form gas cavities extended to the blade surface, the lower pressure regions. Significant peak of kinetic energy is observed near the corner of the dished bottom and its enhancement depends on the impeller speed. The Power number is first decreasing with the Reynolds number and after crossing a particular Reynolds number; it increases very slightly and then finally becomes constant.

REFERENCES

[1] P.H.Calderbank, M.B.Moo-Young; Chem.Eng.Sci., **16**, 39-54 **(1961)**.
[2] D.Chapple, S.M.Kresta, A.Wall, A.Facan; Canada. Chem.Eng.Res.Des., **74(3)**, 617-623 **(2002)**.
[3] H.Deng, R.K.Mehta, G.W.Warren; Int.J.Miner. Process, **48**, 61-72 **(1996)**.
[4] D.A.Deglon, C.J.Meyer; Miner.Eng., **19**, 1059-1068 **(2005)**.
[5] B.K.Gorain, J.P.Franzidis, E.V.Manlapig; Miner. Eng., **9**, 639-654 **(1996)**.
[6] C.K.Harris, D.Roekaerts, F.J.J.Rosendal, F.G.J.Buitendijk, P.H.Daskopoulos, A.J.N.Vreenegoor, H.Wang; Computational Fluid Dynamics for Chemical Reactor Engineering, ISCRE 14, Bruggs, Belgium, **(1996)**.
[7] R.M.Hockey, J.M.Nouri; Chem.Eng.Sci., **51**, 4405-4421 **(1996)**.
[8] P.T.L.Koh, M.P.Schwarz; Miner.Eng., **16**, 1055-1059 **(2003)**.
[9] J.M.Nouri, J.H.Whitelaw; Effects of Size and Confinement on the Flow Characteristics in Stirred Reactors. Proc. 5th Int.Symp.on Applications of Laser Techniques to Fluid Mechanics. Paper 23(2), Lisbon, **(1990)**.
[10] R.Panneerselvam, S.Savithri, G.D.Surender; Chem. Eng.Res.Des., **86**, 1331-1344 **(2008)**.
[11] V.V.Ranade; Rev.Chem.Eng., **11**, 229-284 **(1995)**.
[12] S.Roy, S.Acharya, M.D.Cloeter; Chem.Eng.Sci., **65(10)**, 3009-3024 **(2010)**.
[13] M.Schafer, M.Yianneskis, P.Wachter, F.Durst; AIChE J., **44**, 1233-1246 **(1998)**.
[14] M.M.C.G.Warmoeskerken, J.Speur, J.M.Smith; Chem.Eng.Commun., **25**, 11-29 **(1984)**.